



Dual delivery of carbon monoxide and doxorubicin using haemoglobin-albumin cluster: Proof of concept for well-tolerated cancer therapy

Journal:	<i>Journal of Materials Chemistry B</i>
Manuscript ID	TB-ART-01-2024-000123.R1
Article Type:	Paper
Date Submitted by the Author:	16-Apr-2024
Complete List of Authors:	Ito, Chihiro; Keio University Faculty of Pharmacy Graduate School of Pharmacy Taguchi, Kazuaki; Keio University Faculty of Pharmacy Graduate School of Pharmacy, Yamada, Taiga; Chuo University Faculty of Science and Engineering Graduate School of Science and Engineering Department of Applied Chemistry Hanaya, Kengo; Keio University Faculty of Pharmacy Graduate School of Pharmacy Enoki, Yuki; Keio University Sugai, Takeshi; Keio University Faculty of Pharmacy Graduate School of Pharmacy Komatsu, Teruyuki; Chuo University Faculty of Science and Engineering Graduate School of Science and Engineering, Department of Applied Chemistry Matsumoto, Kazuaki; Keio University

ARTICLE

Dual delivery of carbon monoxide and doxorubicin using haemoglobin-albumin cluster: Proof of concept for well-tolerated cancer therapy

Received 00th January 20xx,
Accepted 00th January 20xx

DOI: 10.1039/x0xx00000x

Chihiro Ito,^a Kazuaki Taguchi,^{*a} Taiga Yamada,^b Kengo Hanaya,^c Yuki Enoki,^a Takeshi Sugai,^c Teruyuki Komatsu,^b and Kazuaki Matsumoto^a

A serious concern of Doxorubicin (DOX) therapy is that it causes severe adverse effects, particularly cardiotoxicity. Carbon monoxide (CO) possesses powerful cytoprotective effects against drug-induced organ injury and is expected to ameliorate DOX-induced cardiotoxicity. In this study, a dual carrier of DOX and CO (CO-HemoAct-DOX) was fabricated based on a haemoglobin-albumin cluster (HemoAct), which is a protein cluster with a haemoglobin core structure wrapped by serum albumin. CO-HemoAct-DOX was synthesised by binding CO to a haemoglobin core and covalently conjugating (6-maleimidocaproyl)hydrazine derivative of DOX to an albumin shell. The average DOX/cluster ratio was about 2.6. In the *in vitro* cytotoxicity assay against cancer cells, the anti-tumour activity of CO-HemoAct-DOX was 10-fold lower than that of DOX in a 2D-cultured model, whereas CO-HemoAct-DOX suppressed the growth of tumour spheroids to the same extent as DOX in the 3D-cultured model. In Colon-26 tumour-bearing mice, CO-HemoAct-DOX achieved DOX delivery to tumour site and alleviated tumour growth more effectively than DOX. Furthermore, CO-HemoAct attenuated DOX-induced cardiomyocyte atrophy in H9c2 cells and elevated the levels of cardiac biomarkers in mice exposed to DOX. These results suggest that the dual delivery of CO and DOX using HemoAct is a promising strategy as an anti-tumour agent to realise well-tolerated cancer therapy with minimal cardiotoxicity.

1. Introduction

Doxorubicin (DOX), an inhibitor of DNA topoisomerase II, is frequently used in cancer therapy and has contributed tremendously to chemotherapy over the past few decades. However, the potent cytotoxicity of DOX causes irreversible and lethal adverse events, particularly cardiotoxicity,¹ leading to a decline in quality of life with unbearable pain and nausea and, in the worst case scenario, discontinuation of chemotherapy. To improve the practical use of DOX, clinicians and researchers have attempted to identify clinical interventions, pharmaceutical agents, and strategies to diminish the incidence of DOX-induced cardiotoxicity.

One strategy to reduce the incidence of DOX-induced cardiotoxicity is to enhance DOX distribution in tumours using drug carriers, including albumin, liposomes, and micelles.^{2–4} These modalities with high molecular weights or nano-sized particles are used to enhance solid tumour accumulation based on a well-established concept for tumour delivery, namely, the enhanced permeability and retention (EPR) effect.⁵ As a matter

of fact, clinically available PEGylated liposomal DOX, Doxil[®], has demonstrated comparable efficacy to DOX and amelioration of cardiotoxicity *in vivo*.⁶ In addition, the (6-maleimidocaproyl)hydrazine derivative of DOX (ALDOX), which binds to endogenous serum albumin after intravenous administration through an acid-sensitive hydrazine linker, exhibits anti-tumour activity with better cardioprotection in pre-clinical and clinical studies.^{7,8} However, it is impossible to deliver the entire amount of DOX to the tumour site even with the use of the carriers, resulting in systemic organ toxicities, including cardiotoxicity. Thus, a novel approach that co-administers organ protectants with DOX is of great interest for systemically suppressing DOX-induced cytotoxicity, and candidates have been found in a wide range of substances, from low- to high-molecular-weight compounds.^{9–11}

Accumulating evidence clearly demonstrates that bioactive gas molecules, such as carbon monoxide (CO), can prevent the onset and progression of organ injuries induced by medicines.^{12–15} In the case of DOX exposure, some reports showed that CO ameliorates DOX-induced cardiotoxicity. Suliman *et al.* showed that CO inhalation prevented DOX-induced cardiomyopathy in mice,¹⁶ and Soni *et al.* showed that concurrent treatments of DOX and CO donor alleviated the elevation of creatine kinase (CK) and lactate dehydrogenase (LDH) in DOX-exposed mice.¹⁷ These facts led us to conclude that materials co-loaded with DOX and CO are well-tolerated DOX preparations with few cardiotoxicities. However, the biological effects of the co-delivery of CO and DOX on

^a Division of Pharmacodynamics, Faculty of Pharmacy, Keio University, 1-5-30 Shibakoen, Minato-ku, Tokyo 105-8512, Japan.

^b Department of Applied Chemistry, Faculty of Science and Engineering, Chuo University, 1-13-27 Kasuga, Bunkyo-ku, Tokyo 112-8551, Japan.

^c Division of Organic and Biocatalytic Chemistry, Faculty of Pharmacy, Keio University, 1-5-30 Shibakoen, Minato-ku, Tokyo 105-8512, Japan.

† Electronic Supplementary Information (ESI) available. See DOI: 10.1039/x0xx00000x

cardiotoxicity have not yet been investigated. To establish a dual delivery system for CO and DOX, we focused on the haemoglobin-albumin cluster (HemoAct), which comprises a haemoglobin core and an albumin shell and was originally developed as artificial blood.^{18,19} As haemoglobin and albumin have potent characteristics for loading CO and drugs, respectively, they have historically been used as carriers of CO and DOX, respectively.^{7,20} In this report, we describe a proof of concept of a dual delivery system of CO and DOX as well-tolerated chemotherapy with low cardiotoxicity. Notably, we synthesised CO- and DOX-loaded HemoAct (CO-HemoAct-DOX) and characterised its physicochemical properties, anti-tumour activity, and cardioprotective effects.

2. Experimental

2.1. Synthesis of CO-HemoAct-DOX

The CO-HemoAct in PBS solution was prepared using carbonyl haemoglobin (COHb) purified from bovine blood (Tokyo Shibaura Zouki Co. Ltd., Tokyo, Japan) coupled with human serum albumin (Japan Blood Products Organisation, Tokyo, Japan) using *N*-succinimidyl 3-maleimidopropionate (SMP), as described previously.¹⁸ A solution of 2-iminothiolane (2-IT) in PBS (20 mM, 1 mL) was added in drops to a solution of CO-HemoAct in PBS ([haemoglobin]=100 μ M, 10 mL) and stirred for 2 h in CO atmosphere under light-shielded conditions at 4 °C. After filtration through the syringe filters (0.22 μ m), unconjugated 2-IT was removed using Sephadex G-25 Superfine (Cytiva) and the total volume was adjusted to 40 mL. 1 mL of ALDOX in DMSO (3.15 mg, 4.2 μ mol), synthesised according to the procedure reported by Willner *et al.*,²¹ was added in drops to the resulting solution and stirred for 1 h in CO atmosphere under light-shielded conditions at 4 °C. To cap the unreacted thiol groups, a solution of *N*-ethylmaleimide (NEM) in PBS (20 mM, 1 mL) was added in drops to the resulting solution and stirred for another 1 h in CO atmosphere under light-shielded conditions at 4 °C. The mixture was concentrated to 10 mL by centrifugation (MWCO: 10 kDa, Amicon® Ultra Centrifugal filters, Merck Millipore), and the unreacted ALDOX and NEM were removed using Sephadex G-25 Superfine. The resulting sample was then concentrated to 4 mL by centrifugation, and CO gas was gently flowed to obtain a solution of CO-HemoAct-DOX in PBS ([haemoglobin]=155 μ M). The concentration of COHb was determined by measuring the absorbance at 419 nm using a UV-vis. spectrophotometer (COHb: $\epsilon_{419} = 7.76 \times 10^5 \text{ M}^{-1} \text{ cm}^{-1}$). The DOX/CO-HemoAct ratio was estimated by fitting and integrating the experimental UV-vis spectra of CO-HemoAct and ALDOX in the range of 450–700 nm using a GRG nonlinear least-squares model with Excel Solver. The samples were stored at 4 °C until further use.

2.2. Characterisation of physicochemical properties of CO-HemoAct-DOX

Dynamic light scattering (DLS) (particle size, polydispersity index, and zeta potential), size exclusion chromatography (SEC), Native-PAGE, isoelectric focusing, and circular dichroism (CD)

were performed under the same experimental conditions as those used in our previous study.²² The detailed methods for each experiment are described in the Supporting Information.

2.3. *In vitro* DOX release from CO-HemoAct-DOX

CO-HemoAct-DOX ([haemoglobin]=50 μ M) in either 200 mM acetate buffer solution (pH 5.5) or 200 mM phosphate buffer solution (pH 6.5 or 7.4) was incubated in a water bath at 37 °C. After 2, 4, 8, 24, and 48 h of incubation, 200 mM phosphate buffer solution (pH 7.4) was added to the sample to quench the reaction. The remaining intact CO-HemoAct-DOX was determined using SEC by monitoring DOX-derived fluorescence (495/550 nm), and the ratio of the released DOX was calculated.

2.4. *In vitro* CO release from CO-HemoAct-DOX

CO-HemoAct-DOX ([haemoglobin]=3.1 μ M) in either 200 mM acetate buffer solution (pH 5.5) or 200 mM phosphate buffer solution (pH 6.5 or 7.4) was incubated at room temperature. At 1, 2, 4, 8, 12, and 24 h after incubation, the absorbance of COHb (419 nm) was determined using a UV-vis spectrometer. The ratio of the released CO was calculated using the following equation:

$$\text{Released CO (\%)} = \{1 - (A_t - A_{\text{baseline}}) / (A_0 - A_{\text{baseline}})\} \times 100$$

where A_t is the absorbance at 419 nm at an individual time point, A_0 is the absorbance at 419 nm before incubation, and A_{baseline} is the absorbance at 419 nm of oxidised HemoAct-DOX, which lost its CO-binding capacity due to the oxidation of ferrous haemoglobin to ferric haemoglobin (methaemoglobin).

2.5. Animals

All animal experiments were approved by the Institutional Animal Care and Use Committee of Keio University (A2022-192). C57BL/6J and BALB/c mice were purchased from Japan SLC, Inc. (Shizuoka, Japan) and acclimatised in a conventional room for at least one week before use in each experiment.

2.6. Biocompatibility evaluation

Male C57BL/6J mice (6- or 7-week-old) were weighed and intravenously injected with either CO-HemoAct-DOX (DOX: 2 mg/kg) or saline *via* the caudal vein. Blood and organs (heart, liver, and kidney) were collected 24 h after test sample injection. The blood was then centrifuged (6000 rpm for 10 min) to obtain plasma samples. Plasma biochemistry levels reflecting heart, liver, and kidney injury (CK, LDH, aspartate transaminase (AST), alanine aminotransferase (ALT), blood urea nitrogen (BUN), and creatinine (CRE)) were measured by Oriental Yeast Industry Co. (Tokyo, Japan). The paraffin-embedded sections (4 μ m-thick) of each organ sample were stained with haematoxylin and eosin to observe morphology using a microscope (BZ-X700, Keyence Corp., Osaka, Japan).

2.7. Biodistribution in healthy mice

C57BL6/J mice (6-week-old, male) were injected with saline, DOX or CO-HemoAct-DOX at a dose of 3 mg DOX/kg *via* the caudal vein. The mice were sacrificed, and blood and organ samples (liver, kidneys, spleen, lungs, and heart) collected at 24

h after sample injection. Fluorescence intensity of the DOX ($\lambda_{\text{ex}}/\lambda_{\text{em}} = 500/620 \text{ nm}$) in plasma and organs were measured by IVIS Lumina LT (PerkinElmer Inc., Waltham, MA, USA). Haemoglobin concentration in plasma was determined using Haemoglobin assay kit (Biochain, Newark, CA, USA).

2.8. Cell viability in monolayer cultured model

Murine colon adenocarcinoma cells (Colon-26 cells, 3×10^3 cells/well), human breast cancer cells (MDA-MB-231 cells, 5×10^3 cells/well; MCF-7 cells, 3×10^3 cells/well), murine melanoma cells (B16F10 cells, 3×10^3 cells/well), human ovarian adenocarcinoma cells (SKOV-3, 3×10^3 cells/well), human gastric carcinoma cells (NCI-N87 cells, 1×10^4 cells/well), human pancreatic cancer cells (AsPC-1 cells, 4×10^3 cells/well), human leukaemia cells (K562 cells, 3×10^3 cells/well) were cultured in 96-well plates for 24 h. Then, the cells were co-cultured with either DOX or CO-HemoAct-DOX for another 48 h. Cell viability was determined using the WST-8 assay (Cell Count Reagent SF; Nacalai Tesque, Kyoto, Japan). Half-maximal inhibitory concentration (IC_{50}) values were calculated based on the survival curves.

2.9. Cytotoxicity assay in Colon-26 and MCF-7 cell spheroids

Spheroids were prepared using a liquid overlay method, as previously described.²³ Colon-26 cells and MCF-7 cells were seeded in an ultra-low attachment 96-well plate (2.5×10^3 cells/well), and the plate was spun for 10 min at 500 rpm. After incubation at 37 °C for 3 days, the spheroids were further co-incubated with DOX or CO-HemoAct-DOX (final concentration; DOX: 0.001–1 μM for Colon-26 cells and DOX: 0.01–10 μM for MCF-7 cells) at 37 °C for 3 days. The spheroid morphology was observed at 100 \times magnification using a microscope (BZ-X700). The cytotoxicity of spheroids treated with DOX or CO-HemoAct-DOX was determined using an acid phosphatase (APH) assay, as reported previously.²⁴

2.10. *In vivo* anti-tumour effects and tumour biodistribution in Colon-26 tumour-bearing mice

Colon-26 cells (2×10^6 cells) were subcutaneously injected into the back of the left femoral area of BALB/c mice (6-week-old males). Colon-26 tumour-bearing mice with tumour size of 50–100 mm^3 were randomised into three groups and intravenously injected with DOX (2 mg/kg), CO-HemoAct-DOX (DOX: 2 mg/kg), or saline once every two days for a total of two doses (on days 0 and 2). The largest length (L) and smallest length (S) of the tumour were measured using a calliper once every 2 days, and the tumour volume (V) was calculated according to the following formula:

$$V = (L \times S^2) / 2$$

All mice were euthanised by cervical dislocation on day 14.

In the biodistribution experiment, Colon-26 tumour-bearing mice with tumour size of approximately 200–300 mm^3 were intravenously injected with DOX (3 mg/kg), CO-HemoAct-DOX (DOX: 3 mg/kg), or saline. After 24 h sample injection, the mice were sacrificed to collect blood and tumour. Fluorescence intensity of the DOX in plasma and tumour were measured by IVIS Lumina LT (PerkinElmer Inc., Waltham, MA, USA).

2.11. Cardiomyocyte atrophy *in vitro*

H9c2 cells (5×10^3 cells/dish) attached to a glass bottom dish ($\phi = 35 \text{ mm}$, Matsunami Glass Industry Co., Ltd., Osaka, Japan) were co-cultured with DOX (1 μM) or a mixture of CO-HemoAct ([haemoglobin]=0.01% or 0.05%) and DOX (1 μM), or CO-HemoAct-DOX ([DOX]=1 μM) for 12 h. After removing the medium, the cells were fixed with 4% paraformaldehyde for 10 min at room temperature and washed three times with PBS. The cells were then permeabilised with 0.1% TritonX-100 for 5 min at room temperature and washed three times with PBS. To visualise F-actin and nuclei, the cells were stained with phalloidin-iFluor 647 reagent (1:2000 dilution, Abcam plc, Cambridge, UK) and DAPI (1:1000 dilution, DOJINDO, Kumamoto, Japan) for 30 min at room temperature. Images of 80 cells from at least ten randomly chosen fields were obtained in three separate experiments using a confocal laser-scanning microscope (FV1000D; Keyence Corp., Osaka, Japan) at 30 \times magnification. The cell surface area was determined using the ImageJ software.

2.12. *In vivo* cardiotoxicity

C57BL/6J mice (9- or 10-week-old females) received either saline, DOX (5 mg/kg), or a mixture of CO-HemoAct (COHb: 1%) and DOX (DOX: 5 mg/kg) *via* the caudal vein once every 2 days for a total of four doses. At 24 h after the final administration of the test solution (day 8), all mice were sacrificed to harvest the heart and blood. The heart was weighed, and blood samples were centrifuged (6000 rpm for 10 min) to obtain plasma. The levels of LDH and CK-MB isoenzyme in plasma were measured using a Fuji DRI-CHEM 7000i (Fujifilm, Tokyo, Japan).

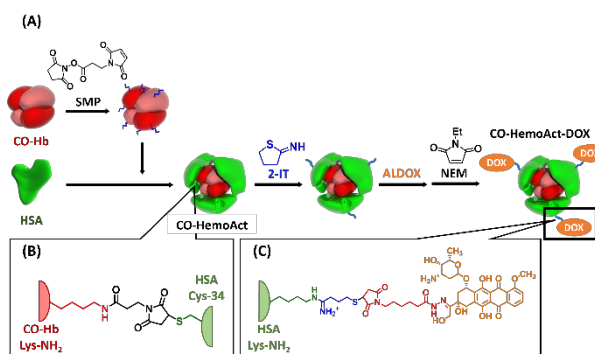
2.13. Statistical analysis

All statistical analyses were performed using the SPSS version 27 software (IBM Corp., Armonk, NY, USA). Multiple comparisons were assessed by one-way analysis of variance (ANOVA) using the Tukey-Kramer test. All data are presented as mean \pm standard deviation (SD) and were considered statistically significant at $p < 0.05$.

3. Results and Discussion

3.1. Synthesis and characteristics of CO-HemoAct-DOX

Similar to a previous report,¹⁹ CO-HemoAct was synthesised by covalently linking haemoglobin and albumin *via* SMP. Thereafter, 2-IT was used to introduce thiol groups into albumin (Scheme 1A). The reason for this treatment was that only the free thiol of albumin (Cys-34), the reaction site of ALDOX, was used to prepare HemoAct (Scheme 1B). After conjugating ALDOX based on the maleimide-thiol reaction, as shown in Scheme 1C, the unreacted thiol groups were capped with NEM because of the possibility of intramolecular disulfide bond formation.²⁵ The as-prepared CO-HemoAct-DOX yielded 75% of the yield of CO-HemoAct. The ratio of CO-HemoAct to DOX was calculated using UV-vis spectroscopy absorption spectra



Scheme 1 (A) Synthetic scheme of CO-HemoAct-DOX. (B) The linker structure between human serum albumin (HSA) and haemoglobin (Hb). (C) The structure of the linker between HSA and DOX.

ranging from 450 to 700 nm, indicating the average DOX/CO-HemoAct ratio was 2.6 ± 0.4 (Figure 1A). As shown in Figure 1B, the cluster size distribution was similar before and after ALDOX conjugation corresponding to an average cluster size of 11.8 ± 0.7 nm and 10.8 ± 0.4 nm for CO-HemoAct-DOX and CO-HemoAct, respectively (Figure 1B). In addition, the polydispersity indexes were also not changed before and after ALDOX conjugation (0.18 ± 0.03 and 0.20 ± 0.02 for CO-HemoAct-DOX and CO-HemoAct, respectively). The particle size and polydispersity indices of CO-HemoAct-DOX were maintained for at least 4 weeks (data not shown). These results suggested that no intramolecular binding or aggregation occurred during the process of ALDOX conjugation or thereafter. The structure of HemoAct revealed that the core of haemoglobin was wrapped with an average of three albumins.^{18,19} Structural differences in CO-HemoAct-DOX were confirmed before and after conjugation with ALDOX. To confirm whether CO-HemoAct-DOX preserved its protein cluster structure, we compared the results of SEC and Native-PAGE between CO-HemoAct-DOX and CO-HemoAct. As shown in Figures 1C and D, no remarkable changes in elution times or band patterns were observed between CO-HemoAct-DOX and CO-HemoAct in SEC and Native-PAGE, respectively. In addition, the CD spectra of CO-HemoAct-DOX and CO-HemoAct were similar (Figure 1E). Furthermore, similar isoelectric point (*pI*) of CO-HemoAct-DOX to that of albumin (*pI*=4.9), but not haemoglobin (*pI*=7.0), indicated that the surface of CO-HemoAct-DOX was covered by albumin (Figure 1F). This speculation was corroborated by the results of zeta-potential (-3.6 ± 0.35 mV and -3.1 ± 0.63 mV for CO-HemoAct-DOX and CO-HemoAct, respectively). These physicochemical results suggest that the cluster structure was maintained in CO-HemoAct-DOX without secondary structural changes in the proteins. The covalent core-shell structure of HemoAct with an albumin-derived surface net charge contributes to good biocompatibility and superior blood retention.^{18,26} In addition, albumin modification on the surface of nanoparticles contributes to their internalisation into tumour cells through caveolae-mediated endocytosis.²⁷ Moreover, their size (*ca.* 10 nm) and negative surface charge met the criteria for displaying EPR effects.²⁸ Therefore, CO-HemoAct-DOX is expected to be a

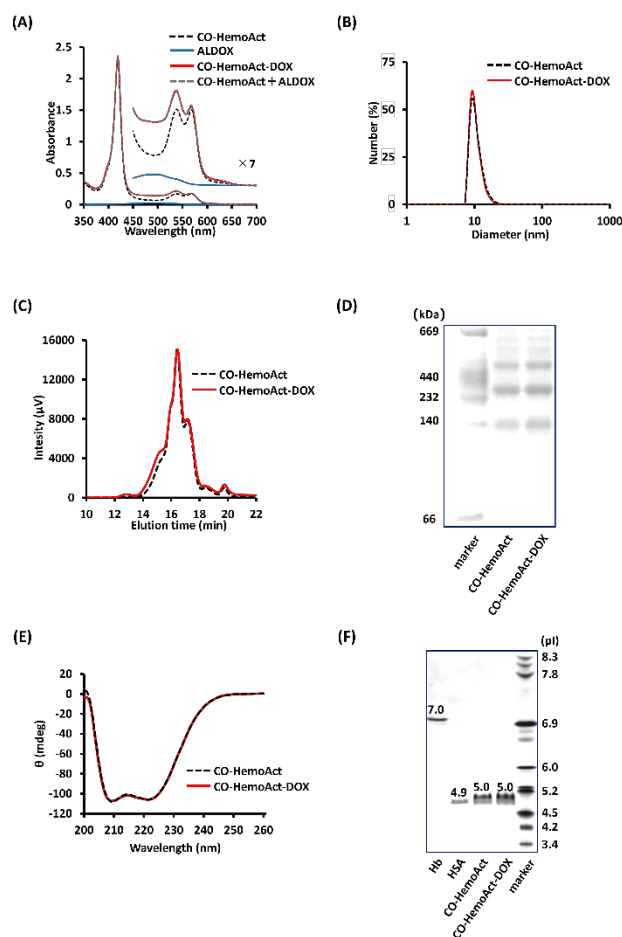


Figure 1 (A) UV-vis spectra, (B) size distribution, (C) size exclusion chromatography, and (D) images of Native-PAGE of CO-HemoAct-DOX and CO-HemoAct. (E) CD spectra of CO-HemoAct-DOX and CO-HemoAct. (F) Image of isoelectric focusing of haemoglobin (Hb), human serum albumin (HSA), CO-HemoAct-DOX and CO-HemoAct. All figures are representative data. Reproducibility was obtained from three independent experiments.

potent anti-tumour agent because of its physicochemical properties.

3.2. DOX- and CO-releasing property of CO-HemoAct-DOX

The peritumoural pH is acidic because of the metabolically produced and diffused protons associated with increased glucose metabolism.²⁹ Thus, we designed a conjugate between CO-HemoAct and DOX through a hydrazone bond to easily release DOX under acidic conditions (Scheme 1C). As expected, the DOX release ratios from CO-HemoAct-DOX in buffer at pH 7.4, 6.5, and 5.5 for 48 h increased as the pH decreased (32.5%, 45.9%, and 68.7% at pH 7.4, 6.5, and 5.5, respectively; Figure 2A). The intracellular lysosomal and endosomal pH in solid tumour is 4.5-5.5.³⁰ These results suggest that CO-HemoAct-DOX releases DOX at tumour sites rather than in normal tissues. We also examined the CO-releasing properties of CO-HemoAct-DOX under various pH conditions. As shown in Figure 2B, the CO release ratios from CO-HemoAct-DOX in buffer at pH 7.4, 6.5, and 5.5 for 24 h were 66.9%, 74.2%, and 90.6%, respectively.

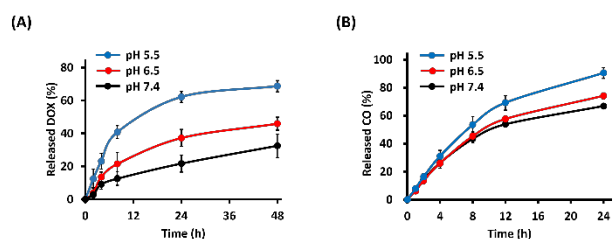


Figure 2 (A) DOX and (B) CO releasing profiles from CO-HemoAct-DOX at pH 5.5, 6.5 and 7.4. Data are represented the mean \pm S.D. (n=3-4).

These results suggest that CO-HemoAct-DOX possesses favourable DOX- and CO-releasing properties.

3.3. Biological compatibility and biodistribution of CO-HemoAct-DOX

Biological compatibility is an essential criterion for pharmaceutical preparations. In the case of CO-HemoAct-DOX, a possible biological incompatibility is DOX-induced heart injury. In addition, its influence on the liver and kidney is also a concern because the liver and kidney are the main organs involved in the metabolism and excretion of HemoAct.¹⁹ Hence, we evaluated the toxicity of CO-HemoAct-DOX in the heart, liver, and kidneys *in vivo*. Table 1 shows biochemical parameters reflecting heart, liver, and kidney injury 24 h after administration of saline (control) or CO-HemoAct-DOX in healthy mice. No significant differences in biochemical parameters were observed among the groups. No abnormal histological changes were observed (Figure S1). These results suggest that CO-HemoAct-DOX has good biological compatibility.

As shown in Figures 3A and B, the fluorescence intensity and visual red colour were observed in the plasma at 24 h after injection of CO-HemoAct-DOX while fluorescence intensity was nearly zero without red colour after the injection of DOX alone. In addition, haemoglobin was detected in plasma samples collected from mice administered CO-HemoAct-DOX (Figure S2A). It was reported that haemoglobin disappeared within a few hours while HemoAct had long blood retention.¹⁹ Hence, haemoglobin detected in plasma would be derived from the haemoglobin of CO-HemoAct-DOX, suggesting that CO-HemoAct-DOX circulated in the bloodstream in intact form (cluster structure with DOX load). In the biodistribution tests, strong fluorescence intensity was observed in the liver after the CO-HemoAct-DOX injection compared to the DOX injection (Figures 3B and S2B). Biodistribution in other organs was not significantly different between DOX and CO-HemoAct-DOX. As some protein formulations that albumin dominates its pharmacokinetics distributed and metabolized in the liver,^{31,32} the liver would be a predominant organ for CO-HemoAct-DOX metabolism.

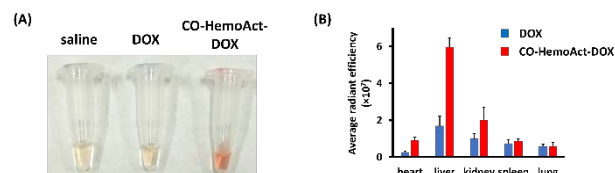


Figure 3 (A) The appearance of plasma at 24h after saline, DOX, and CO-HemoAct-DOX administration. (B) The fluorescence intensity of isolated organs collected from healthy mice administered either DOX or CO-HemoAct-DOX. Each column represents the mean \pm S.D. (n=5).

3.4. Cytotoxicity of CO-HemoAct-DOX against 2D-cultured cancer cell lines

We evaluated the cytotoxicity of CO-HemoAct-DOX against eight cancer cell lines derived from colon adenocarcinoma (Colon-26 cells), breast cancer (MCF-7 and MDA-MB-231 cells), melanoma (B16F10 cells), ovarian adenocarcinoma (SKOV-3 cells), gastric carcinoma (NCI-N87 cells), pancreatic cancer (AsPC-1 cells), and leukaemia (K562 cells). CO-HemoAct-DOX exhibited dose-dependent cytotoxicity in all cancer cell lines (Figure S3). However, the IC_{50} value of CO-HemoAct-DOX was 6.9-15-fold less than those of DOX (Table 2). Because the anti-tumour effect of CO has been reported in some types of cancer,³³⁻³⁵ we also investigated the effect of CO-HemoAct on cancer cells. No CO-HemoAct cytotoxicity was observed in any of the cancer cell lines used in this study (data not shown), suggesting that the cytotoxicity of CO-HemoAct-DOX against 2D-cultured cancer cells was attributed to DOX.

3.5. Cytotoxicity of CO-HemoAct-DOX against 3D-cultured Colon-26 and MCF-7 cells

Besides the 2D-cultured model, we also assessed the cytotoxicity of CO-HemoAct-DOX against a 3D-cultured model, which mimicked the tumour environment *in vivo*.³⁶ Compared to the control spheroids of Colon-26 and MCF-7 cells, the growth of spheroids was visually suppressed by CO-HemoAct-DOX, similar to DOX on day 3 (Figures 4A and B). Consistent with the imaging results, quantitative analysis (APH assays) showed that CO-HemoAct-DOX was cytotoxic against both tumour spheroids to the same extent as DOX (Figures 4C and D), even though the cytotoxicity of CO-HemoAct-DOX was 10- and 14.3-fold lower than that of DOX in 2D-cultured Colon-26 and MCF-7 cells, respectively (Table 2). According to a previous report, negatively charged nanoparticles can easily penetrate the core of tumour spheroids.³⁷ Hence, CO-HemoAct-DOX may penetrate the core of tumour spheroids and be gradually taken up by tumour cells, suggesting that CO-HemoAct-DOX can strongly inhibit tumour growth *in vivo*.

Table 1 Biochemical parameters at 24 h after administration of CO-HemoAct-DOX (DOX: 2 mg/kg, COHb: 1%) or saline in healthy mice. Data are represented as mean \pm S.D. (n=5). CK, creatine kinase; LDH, lactate dehydrogenase; AST, aspartate transaminase; ALT, alanine aminotransferase; BUN, blood urea nitrogen; CRE, creatinine.

	CK (IU/L)	LDH (IU/L)	AST (IU/L)	ALT (IU/L)	BUN (mg/dL)	CRE (mg/dL)
saline	84.8 \pm 13.0	131.8 \pm 12.6	29.0 \pm 5.8	18.0 \pm 10.3	23.5 \pm 0.8	0.078 \pm 0.007
CO-HemoAct-DOX	63.4 \pm 14.5	143.6 \pm 7.8	32.6 \pm 4.0	18.2 \pm 2.8	30.4 \pm 3.2	0.10 \pm 0.01

Table 2 IC₅₀ values of CO-HemoAct-DOX and DOX against cancer cell lines.

	IC ₅₀ (μM of DOX equivalent)	
	CO-HemoAct-DOX	DOX
Colon-26	2.1	0.21
MCF-7	4.3	0.30
MDA-MB-231	5.6	0.81
B16F10	1.3	0.093
SKOV-3	3.5	0.49
NCI-N87	6.0	0.40
AsPC-1	20.8	2.16
K562	0.30	0.042

3.6. Anti-tumour effect and tumour distribution of CO-HemoAct-DOX against Colon-26 tumour-bearing mice

The anti-tumour effect of CO-HemoAct-DOX was evaluated in Colon-26 tumour-bearing mice. Although the *in vitro* anti-tumour effect of CO-HemoAct-DOX in 2D- and 3D-cultured Colon-26 cells was similar to that of DOX (Figure 4 and Table 2), CO-HemoAct-DOX inhibited the growth of Colon-26 tumours *in*

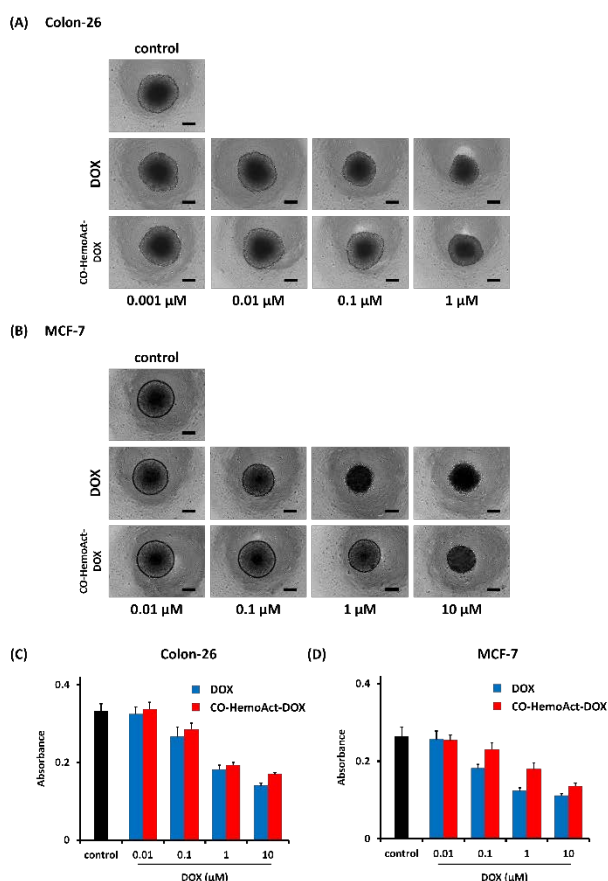


Figure 4 Cell morphology of (A) Colon-26 spheroids and (B) MCF-7 spheroids treated with DOX or CO-HemoAct-DOX on day 3. Scale bar: 200 μm. APH activities of (C) Colon-26 spheroids and (D) MCF-7 spheroids treated with DOX or CO-HemoAct-DOX on day 3. Data are represented as mean ± S.D. (n=4).

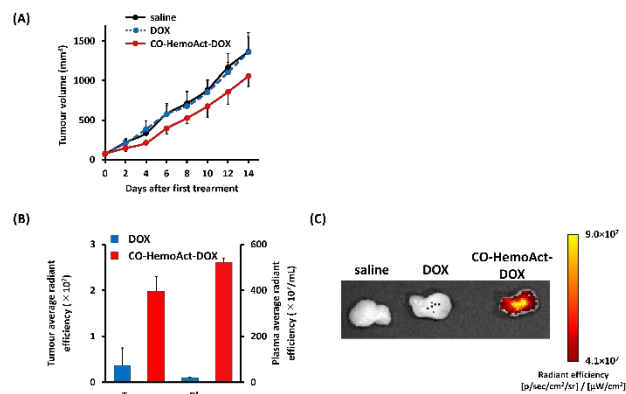


Figure 5 (A) Changes in tumour volume of Colon-26 tumour-bearing mice after treatments with DOX, CO-HemoAct-DOX, or saline (control). Data are represented as mean ± S.D. (n=6). (B) Fluorescence intensity in tumour and plasma collected from Colon-26 tumour-bearing mice at 24 h after DOX and CO-HemoAct-DOX injection. Data are represented as mean ± S.D. (n=3). (C) *Ex vivo* fluorescence image in tumour after saline, DOX, and CO-HemoAct-DOX injection.

in vivo at an equivalent DOX dose at which DOX did not exhibit any anti-tumour effect (Figure 5A). Nanomedicines that have optimized size (less than 200 nm), negative charge, good biological compatibility, and long blood retention display a strong EPR effect.²⁸ Based on the aforementioned results, CO-HemoAct-DOX has *ca.* 10 nm in size with a negative charge (Figure 1B), good biological compatibility (Table 1), and long blood retention (Figures 3A and S2). Thus, the gap in anti-tumour efficacy between *in vitro* and *in vivo* studies could be due to the effective DOX delivery by CO-HemoAct-DOX to the tumour site through the EPR effect. To demonstrate this, we compared the tumour distribution of DOX and CO-HemoAct-DOX by monitoring DOX-derived fluorescence. As shown in Figures 5B and C, higher fluorescence intensity in the tumour was observed in Colon-26 tumour-bearing mice administered CO-HemoAct-DOX than in those administered DOX, suggesting that much more DOX accumulated in the tumour after CO-HemoAct-DOX administration compared to DOX administration. Additionally, the strong fluorescence intensity derived from DOX and high haemoglobin concentration with visual red colour was observed in the plasma of Colon-26 tumour-bearing mice at 24 h after CO-HemoAct-DOX administration (Figures 5B and S4). On the other hand, these alterations in plasma are not observed in Colon-26 tumour-bearing mice administered DOX (Figures 5B and S4). Hence, CO-HemoAct-DOX could effectively deliver DOX to the tumour site owing to its superior passive targeting properties. Fang *et al.* reported that exogenous CO functions as an EPR enhancer, resulting in the augmented anti-tumour effects of nanodrugs.³⁸ In addition, albumin is known to pass through the endothelial barrier at the tumour site *via* albumin-binding proteins such as Gp60.^{39,40} Since tumour tissues consume a great deal of nutrients and energy during the rapid growth of tumour cells, albumin appears to be taken up as a source of nutrients *via* albumin-binding proteins.⁴⁰ Therefore, CO-HemoAct-DOX, whose surface was covered by albumin, with a core haemoglobin load (CO), could be effectively delivered to tumour tissues by enhancing the EPR effect and uptake *via* Gp60, leading to high anti-tumour activity.

3.7. Protective effect of CO-HemoAct against DOX-induced cardiotoxicity

Administration of DOX induces cardiotoxicity, such as cardiomyocyte atrophy and elevated cardiac biomarker levels. As some studies have shown that CO supplied from CORMs, which are chemically synthesised CO-releasing molecules, ameliorates DOX-induced cardiotoxicity,^{17,41} the cardioprotective effect of CO-HemoAct-DOX was evaluated *in vitro* and *in vivo*. Given the different behaviours between DOX and DOX derived from CO-HemoAct-DOX, it is difficult to determine whether the cardioprotective mechanism of CO-HemoAct-DOX is because of CO supplied from CO-HemoAct-DOX that protects against cardiotoxicity or the sustained DOX released from CO-HemoAct-DOX that suppresses the induction of cardiotoxicity. Hence, we compared the induction of cardiotoxicity between DOX treatments with or without CO-HemoAct *in vitro* and *in vivo* to exclude the effects of the distinct DOX concentration profiles between DOX and CO-HemoAct-DOX.

In *in vitro* assay, cardiomyocytes (H9c2 cells) were exposed to DOX with or without CO-HemoAct and assessed for DOX-induced cardiomyocyte atrophy. As shown in Figure 6A, cardiomyocyte atrophy was visually observed after DOX exposure but was suppressed by co-incubation with 0.05% CO-HemoAct. The quantitative analysis of the cardiomyocyte atrophy clearly showed that the mean cell area of each cardiomyocyte decreased after DOX exposure (Figure 6B;

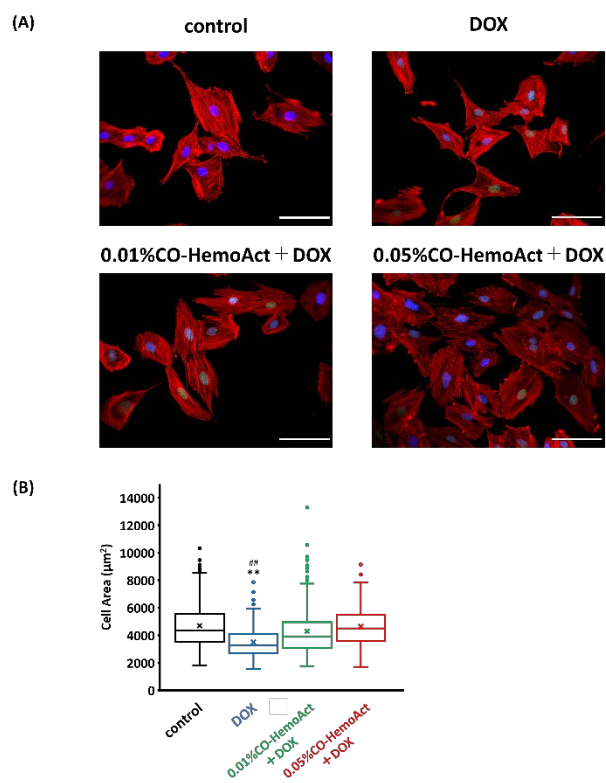


Figure 6 (A) Morphology and (B) cell area of H9c2 cell after DOX treatment with or without CO-HemoAct. Scale bar: 100 µm. Data are represented as mean \pm S.D. (n=3). ** p <0.01 versus control, ## p <0.01 versus 0.05%CO-HemoAct+DOX.

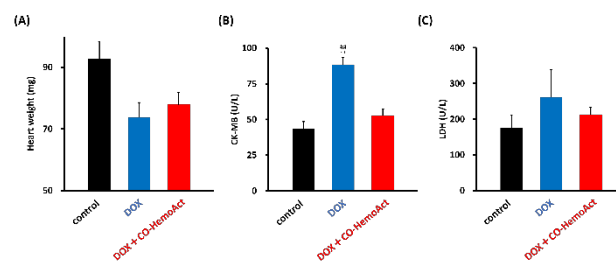


Figure 7 (A) Heart weight, (B) CK-MB, and (C) LDH in healthy mice after DOX treatment with or without CO-HemoAct. Data are represented as mean \pm S.D. (n=6). ** p <0.01 versus control, ## p <0.01 versus DOX+CO-HemoAct.

4699.6 \pm 109.7 and 3514.5 \pm 173.9 μm^2 for control and DOX, respectively, p <0.01), and co-incubation with CO-HemoAct suppressed cardiomyocyte atrophy, and DOX with 0.05% CO-HemoAct group recovered cell area to the level of the control group (Figure 6B; 3930.4 \pm 101.9 and 4647.4 \pm 81.9 μm^2 for DOX with 0.01% and 0.05% CO-HemoAct, respectively). Note that CO-HemoAct-DOX (DOX: 1 μM) did not show the cardiomyocyte atrophy (Figure S5). These results suggest that CO-HemoAct-DOX can attenuate DOX-induced cardiomyocyte atrophy *via* the CO supply.

We further investigated the cardioprotective effects of CO-HemoAct *in vivo* by comparing cardiac injury markers after repeated DOX exposure with or without CO-HemoAct. The heart weight was slightly increased, but not significantly, by the co-administration of DOX and CO-HemoAct (Figure 7A). However, the increase in CK-MB and LDH levels after repeated DOX exposure was suppressed by co-administration with CO-HemoAct (Figures 7B and C), implying that CO-HemoAct could reduce the risk of heart injury. Kim *et al.* revealed that CO inhibits caspase-3 activation in H9c2 cells *via* elevating Bcl-2 expression and suppressing Bax expression, resulting in the inhibition of DOX-induced cardiomyocyte death.⁴¹ Soni *et al.* showed that CO protects against DOX-induced cardiotoxicity in mice through its antioxidant and antiapoptotic properties.¹⁷ Considering the versatile bioactivities of CO,⁴² the CO supplied by CO-HemoAct would contribute to cardioprotection *via* antioxidative and anti-apoptotic effects. Further detailed research is warranted to demonstrate the cardioprotective mechanism of CO-HemoAct.

4. Conclusions

CO-HemoAct-DOX was synthesised by covalently conjugating DOX to an albumin shell *via* an acid-sensitive linker and non-covalently binding CO to the haemoglobin core of HemoAct. DOX and CO did not influence cluster or protein structure and were released in response to the acidic environment. CO-HemoAct-DOX suppressed the growth of various types of 2D-cultured cancer cell lines; however, its anti-tumour activity was inferior to that of DOX. Notably, CO-HemoAct-DOX inhibited tumour growth in Colon-26 tumour-bearing mice better than DOX. Furthermore, CO supplied by CO-HemoAct-DOX ameliorated DOX-induced cardiotoxicity. These results suggest that CO-HemoAct-DOX is a novel DOX preparation with low cardiotoxic effects. In addition, the co-delivery of anticancer

agents and CO using nanocarriers is a promising strategy for the development of anti-tumour agents with few adverse effects.

Conflicts of interest

There are no conflicts to declare.

Acknowledgements

This study was financially supported by the Mochida Memorial Foundation for Medical and Pharmaceutical Research and JST SPRING (grant number JPMJSP2123).

References

- I. C. Jones and C. R. Dass, *J. Pharm. Pharmacol.*, 2022, **74**, 1677–1688.
- M. Gyöngyösi, D. Lukovic, K. Zlabinger, A. Spannauer, A. Gugerell, N. Pavo, D. Traxler, D. Pils, G. Maurer, A. Jakab, M. Riesenhuber, A. Pircher, J. Winkler and J. Bergler-Klein, *Cardiovasc Res.*, 2020, **116**, 970–982.
- N. A. D'Angelo, M. A. Noronha, M. C. C. Câmara, I. S. Kurnik, C. Feng, V. H. S. Araujo, J. H. P. M. Santos, V. Feitosa, J. V. D. Molino, C. O. Rangel-Yagui, M. Chorilli, E. A. Ho and A. M. Lopes, *Biomater Adv.*, 2022, **133**, 112623.
- K. Kimura, K. Yamasaki, K. Nishi, K. Taguchi and M. Otagiri, *Cancer Chemother. Pharmacol.*, 2019, **83**, 1113–1120.
- H. Maeda, K. Tsukigawa and J. Fang, *Microcirculation*, 2016, **23**, 173–182.
- A. Gabizon, H. Shmeeda and Y. Barenholz, *Clin. Pharmacokinet.*, 2003, **42**, 419–436.
- L. D. Cranmer, *Onco Targets Ther.*, 2019, **12**, 2047–2062.
- F. Kratz, A. Warnecke, K. Scheuermann, C. Stockmar, J. Schwab, P. Lazar, P. Drückes, N. Esser, J. Drevs, D. Rognan, C. Bissantz, C. Hinderling, G. Folkers, I. Fichtner and C. Unger, *J Med Chem*, 2002, **45**, 5523–5533.
- L. Yang, J. Guan, S. Luo, J. Yan, D. Chen, X. Zhang, C. Zhong and P. Yang, *Toxicol. Appl. Pharmacol.*, 2023, **479**, 116713.
- S. Wei, W. Ma, Y. Yang, T. Sun, C. Jiang, J. Liu, B. Zhang and W. Li, *Biochem. Pharmacol.*, 2023, **214**, 115662.
- D. Fan, Z. Jin, J. Cao, Y. Li, T. He, W. Zhang, L. Peng, H. Liu, X. Wu, M. Chen, Y. Fan, B. He, W. Yu, H. Wang, X. Hu and Z. Lu, *Redox Biol.*, 2023, **64**, 102780.
- Y. Xue, D. Zhang, Y. Wei, C. Guo, B. Song, Y. Cui, C. Zhang, D. Xu, S. Zhang and J. Fang, *Eur. J. Pharm. Sci.*, 2023, **184**, 106413.
- Z. Xia, C. Zhang, C. Guo, B. Song, W. Hu, Y. Cui, Y. Xue, M. Xia, D. Xu, S. Zhang and J. Fang, *Acta Biomater.*, 2022, **144**, 42–53.
- K. Taguchi, Y. Suzuki, M. Tsutsuura, K. Hiraoka, Y. Watabe, Y. Enoki, M. Otagiri, H. Sakai and K. Matsumoto, *Pharmaceutics*, 2021, **14**, 57.
- T. Nagasaki, H. Maeda, H. Yanagisawa, K. Nishida, K. Kobayashi, N. Wada, I. Noguchi, R. Iwakiri, K. Taguchi, H. Sakai, J. Saruwatari, H. Watanabe, M. Otagiri and T. Maruyama, *Antioxidants*, 2023, **12**, 1705.
- H. B. Suliman, M. S. Carraway, A. S. Ali, C. M. Reynolds, K. E. Welty-Wolf and C. A. Piantadosi, *J. Clin. Invest.*, 2007, **117**, 3730–3741.
- H. Soni, G. Pandya, P. Patel, A. Acharya, M. Jain and A. A. Mehta, *Toxicol. Appl. Pharmacol.*, 2011, **253**, 70–80.
- R. Funaki, T. Kashima, W. Okamoto, S. Sakata, Y. Morita, M. Sakata and T. Komatsu, *ACS Omega*, 2019, **4**, 3228–3233.
- R. Haruki, T. Kimura, H. Iwasaki, K. Yamada, I. Kamiyama, M. Kohno, K. Taguchi, S. Nagao, T. Maruyama, M. Otagiri and T. Komatsu, *Sci. Rep.*, 2015, **5**, 12778.
- K. Taguchi, T. Maruyama and M. Otagiri, *Curr. Med. Chem.*, 2018, **27**, 2949–2963.
- D. Willner, P. A. Trail, S. J. Hofstead, H. Dalton King, S. J. Lasch, G. R. Braslawsky, R. S. Greenfield, T. Kaneko and R. A. Firestone, *Bioconjug. Chem.*, 1993, **4**, 521–527.
- Y. Suzuki, K. Taguchi, W. Okamoto, Y. Enoki, T. Komatsu and K. Matsumoto, *J. Control. Release*, 2022, **349**, 304–314.
- C. Ito, K. Taguchi, Y. Moroi, Y. Enoki, R. Tokuda, K. Yamasaki, S. Imoto and K. Matsumoto, *J. Pharm. Sci.*, 2022, **111**, 2201–2209.
- Y. Okamoto, K. Taguchi, S. Imoto, V. T. Giam Chuang, K. Yamasaki and M. Otagiri, *J. Drug Deliv. Sci. Technol.*, 2020, **55**, 101381.
- K. Yasuda, H. Maeda, R. Kinoshita, Y. Minayoshi, Y. Mizuta, Y. Nakamura, S. Imoto, K. Nishi, K. Yamasaki, M. Sakuragi, T. Nakamura, M. Ikeda-Imafuku, Y. Iwao, Y. Ishima, T. Ishida, Y. Iwakiri, M. Otagiri, H. Watanabe and T. Maruyama, *ACS Nano*, 2023, **17**, 16668–16681.
- W. Okamoto, M. Hasegawa, T. Usui, T. Kashima, S. Sakata, T. Hamano, H. Onozawa, R. Hashimoto, M. Iwazaki, M. Kohno and T. Komatsu, *J. Biomed. Mater. Res. B Appl. Biomater.*, 2022, **110**, 1827–1838.
- M. Sousa De Almeida, E. Susnik, B. Drasler, P. Taladriz-Blanco, A. Petri-Fink and B. Rothen-Rutishauser, *Chem. Soc. Rev.*, 2021, **50**, 5397–5434.
- H. Maeda, H. Nakamura and J. Fang, *Adv. Drug Deliv. Rev.*, 2013, **65**, 71–79.
- P. A. Schornack and R. J. Gillies, *Neoplasia*, 2003, **5**, 135–145.
- K. Zhang, P. P. Yang, J. P. Zhang, L. Wang and H. Wang, *Chin. Chem. Lett.*, 2017, **28**, 1808–1816.
- K. Taguchi, H. Lu, Y. Jiang, T. T. Hung and M. H. Stenzel, *J. Mater. Chem. B*, 2018, **6**, 6278–6287.
- K. Taguchi, V. T. G. Chuang, K. Yamasaki, Y. Urata, R. Tanaka, M. Anraku, H. Seo, K. Kawai, T. Maruyama, T. Komatsu and M. Otagiri, *J Pharm Pharmacol.*, 2015, **67**, 255–263.
- K. Krukowska and M. Magierowski, *Biochem Pharmacol*, 2022, **201**, 115058.
- J. Chai, J. Zhu, Y. Tian, K. Yang, J. Luan and Y. Wang, *J. Mater. Chem. B*, 2023, **11**, 1849–1865.
- Y. Zhou, W. Yu, J. Cao and H. Gao, *Biomaterials*, 2020, **255**, 120193.
- H. Lu and M. H. Stenzel, *Small*, 2018, **14**, 1702858.
- A. Tchoryk, V. Taresco, R. H. Argent, M. Ashford, P. R. Gellert, S. Stolnik, A. Grabowska and M. C. Garnett, *Bioconjug. Chem.*, 2019, **30**, 1371–1384.
- J. Fang, R. Islam, W. Islam, H. Yin, V. Subr, T. Etrych, K. Ulbrich and H. Maeda, *Pharmaceutics*, 2019, **11**(7), 343.
- P. J. Pan and J. X. Liu, *World J Clin Cases*, 2021, **9**, 6287–6299.
- P. Zhao, Y. Wang, A. Wu, Y. Rao and Y. Huang, *ChemBioChem*, 2018, **19**, 1796–1805.
- D. S. Kim, S. W. Chae, H. R. Kim and H. J. Chae, *Immunopharmacol. Immunotoxicol.*, 2009, **31**, 64–70.
- R. Motterlini and L. E. Otterbein, *Nat. Rev. Drug Discov.*, 2010, **9**, 728–743.